

## Evaluation of the dose variation for prostate heavy charged particle therapy using four-dimensional computed tomography

Motoki KUMAGAI, Tohru OKADA, Shinichiro MORI\*, Susumu KANDATSU and Hiroshi TSUJI

Research Center for Charged Particle Therapy, National Institute of Radiological Sciences, Anagawa 4-9-1, Inage, Chiba 263-8555, Japan

\*Corresponding author. Tel: +81-43-251-2111; Fax: +81-43-284-0198; Email: shinshin@nirs.go.jp

(Received 2 November 2011; revised 11 October 2012; accepted 11 October 2012)

We quantified dose variation effects due to respiratory-induced intrafractional motion in conventional carbon-ion prostate treatment by using four-dimensional computed tomography (4DCT). 4DCT scans of 20 patients were acquired under free-breathing conditions using a 256 multi-slice CT scanner. The clinical target volume (CTV) was defined as the prostate and the seminal vesicle. Two types of planning target volumes (PTVs) were defined to minimize excessive dose to the rectum. The first PTV (= PTV1) was calculated by adding a 3D uniform margin to the CTV. The second PTV (= PTV2) was cut in a straight line from the top surface of the rectum from PTV1. Compensating boli were designed for the respective PTVs at the peak-exhalation phase, and carbon-ion dose distributions for a single respiratory cycle were calculated using these boli. Dose conformation to prostate, CTV, PTV1 and PTV2 were unchanged for all respiratory phases. The dose for >95% volume irradiation (D95) was 97.7% for prostate, 92.5% for CTV, 74.1% for PTV1 and 96.1% for PTV2 averaged over all patients. The rectum volume at inhalation phase receiving  $\leq 50\%$  of the prescribed dose was smaller than the planning dose due to the abdominal thickness variation. The target dose is not affected by intrafractional respiration in carbon-ion prostate treatment. Small dose variations, however, were observed due to respiratory-induced abdominal thickness variation; therefore the geometrical changes should be considered for prostate particle therapy.

**Keywords:** charged particle therapy; 4DCT; intrafractional motion; prostate

### INTRODUCTION

Prostate treatment by charged particles offers a high conformity due to their characteristic depth dose distribution known as the Bragg peak. This results in good local control with minimal dosages to the surrounding normal tissue [1, 2]. To benefit maximally from a highly conformal treatment, precise knowledge of the tumor position and its adjacent organs at risk (OAR), such as the rectum, is mandatory.

Several studies have reported on intra- and inter-fractional prostate motion by using various types of imaging systems [3–10]. Intrafractional motion and inter-fractional changes, however, remain a fundamental challenge in thoracic and abdominal treatments. ‘Intrafractional tumor motion can be of two types: stochastic (i.e. random in time and direction) and systematic. Systematic motion can consist of slow, quasi-static changes in position due to

effects such as muscle fatigue as well as rapid, cyclic changes caused by respiration and heart beat’, as defined by Murphy [11]. Respiratory motion changes anatomical and tumor position as a function of time. As a result the tumor moves out of the treatment beam field and hence the dose to normal tissues is increased.

To our knowledge, the dosimetric effect due to intrafractional motion has not yet been evaluated for prostate therapy using a carbon-ion beam. Recently new treatment techniques aiming to further improve target conformity have been developed, namely ‘scanning’ and ‘layer-stacking’ [12–14]. Their application to moving tumors is currently under research [12, 13]. In order to set up a clinical treatment protocol for these new delivery modalities the dose variation due to organ motion needs to be quantified for the conventional therapy. Our institution uses a carbon-ion beam for prostate therapy under free-breathing conditions. It may be affected by intrafractional motion because

of its high conformity. In this paper we evaluated the dose variation for conventional passive carbon-ion beam therapy using 4DCT data sets.

## MATERIALS AND METHODS

### Patient selection

Twenty patients between 57 and 76 years (mean, 66.7 years; SD, 5.5 years) were randomly selected from a group of patients suffering from prostate cancer. All of them consented to participate in this study, which was approved by the Institutional Review Board of the National Institute of Radiological Sciences (NIRS). Patient characteristics are summarized in Table 1.

### 4DCT data acquisition

According to our prostate treatment protocol, the bladder was filled with 100 ml of sterilized water and the rectum was emptied by the patient's effort or a laxative or enema.

**Table 1.** Summary of patient characteristics, respiratory cycle and center of mass (COM) displacement

Pt. no.	Age (y)	T stage	Respiratory cycle (s)	COM (mm)
1	59	T3aN0M0	3.4	0.1
2	71	T3bN0M0	4.0	0.1
3	58	T1cN0M0	2.6	0.0
4	71	T2aN0M0	4.2	0.1
5	65	T2aN0M0	4.3	0.5
6	76	T2aN0M0	4.0	0.2
7	63	T2bN0M0	3.6	0.3
8	76	T3aN0M0	3.2	0.2
9	63	T1cN0M0	2.9	0.5
10	67	T1cN0M0	3.3	0.3
11	57	T2aN0M0	3.3	0.7
12	68	T1cN0M0	3.3	0.5
13	67	T2bN0M0	5.2	0.2
14	67	T1cN0M0	4.0	0.4
15	74	T3aN0M0	3.9	0.0
16	61	T2bN0M0	2.5	0.2
17	67	T2aN0M0	3.4	0.1
18	65	T3aN0M0	3.7	0.4
19	68	T1cN0M0	3.4	0.1
20	70	T3bN0M0	4.3	0.2
Mean	66.7		3.6	0.3
s.d.	5.5		0.6	0.2

Pt. no. = patient number.

This was done for the planning CT as well as for each treatment stage in order to achieve a consistent tumor positioning and hence minimize dose variation between planning and the actual treatment delivery. The 4DCT acquisition was done immediately after the irradiation to ensure the same patient conditions such as bladder filling and rectum position etc. Each patient lay on the CT couch in supine position and was kept immobile using a low-temperature thermoplastic device (Shellfitter; Keraray Co., Ltd, Osaka, Japan), which has a relatively thick shell (3 mm). The respiratory signals were acquired by a respiratory-sensing system (Toyonaka Kenkyujo, Osaka, Japan). An infrared-emitting light marker was positioned on the abdomen region outside the beam field. Its motion was detected by a position-sensitive detector sensor.

The 4DCT was acquired under free-breathing conditions using a 256-multislice CT (256MSCT) (Fig. 1a) [15, 16]. The slice collimation was  $128 \times 1.0$  mm and the rotation time was 0.5 s/rotation; the image reconstruction was done at  $512 \times 512 \times 128$  voxels leading to a voxel size of  $0.78$  mm  $\times$   $0.78$  mm  $\times$   $1.0$  mm. The scan time was set to cover a single respiratory cycle (less than 6 s). A summary of the respiratory parameters during 4DCT is shown in Table 1. The 4DCT data set was equally subdivided into 10 phases (T00: peak-inhalation, T30: mid-exhalation, T50: peak-exhalation) based on the respiratory signal amplitude [17, 18].

### Target definition

Prostate, seminal vesicle and rectum were manually contoured on the CT images at each respiratory phase by a certified radiation oncologist (Fig. 1b). To minimize delineation errors of the organs, additional MRI images were used. The images were compared without registration but on the same display [19, 20]. The clinical target volume (CTV) was defined as the prostate and the seminal vesicle. Two types of planning target volumes (PTVs) were defined. The initial PTV (PTV1) was defined by adding 10 mm to the anterior and lateral sides and 5 mm to the posterior side of the CTV. These margins account for setup errors and errors due to interfractional positional changes (= internal margin: IM). They were not derived from the 4DCT but set constant because our prostate routine treatment protocol does not use 4DCT. The PTV2 was cut in a straight line under the posterior side from the PTV1 to avoid excessive dose to the rectum; the cutline was defined by the anterior rectum wall [21].

### Abdominal thickness

The abdominal thickness was calculated as the water equivalent path length (WEL) from the anterior skin surface to the distal edge of the PTV1 as a function of respiratory phase. Our assessment of abdominal thickness did not include the immobilization devices. We chose a region of interest (ROI) evaluation approach to minimize

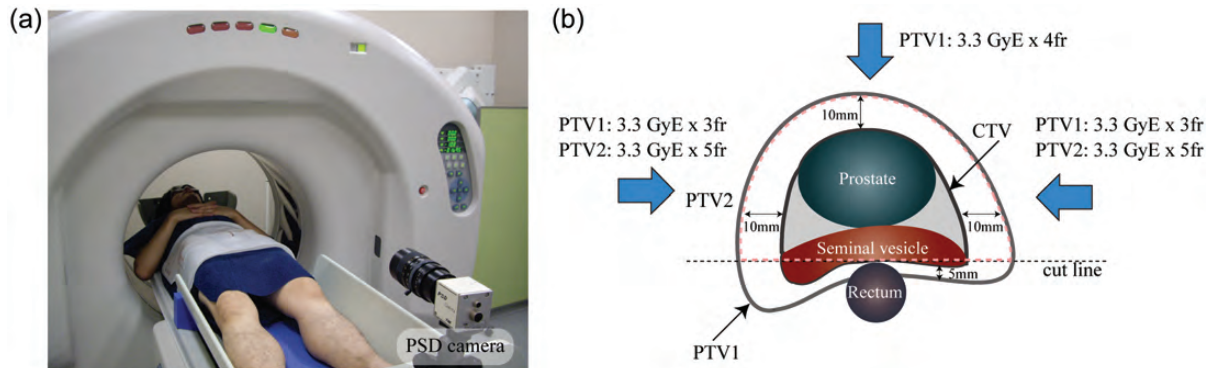


**Fig. 1.** (a) Prostate 4DCT front view. (b) Schematic drawing of the contours. The clinical target volume (CTV) includes the prostate and the seminal vesicle. Initial planning target volume (= PTV1) was defined by adding a margin (10 mm to the anterior and lateral sides and 5 mm to the posterior side of the CTV) to the CTV. The second PTV (PTV2) was defined by reducing the posterior margin from PTV1 to decrease the dose to the rectum. CTV = clinical target volume, PTV = planning target volume.

uncertainty from local variations and uncertainties in individual line placement. We set the ROI (= ROI1) projected region over the PTV1 from the anterior side. Two other circular ROIs (= 10 mm diameter) were set on the 0.7 cm inner side from the PTV1 superior side (= ROI2) and on the 0.7 cm inner side from the inferior side of the PTV1 (= ROI3). Abdominal thickness was quantified over the ROIs from the anterior direction.

### Treatment planning and dose assessment

We used the peak-exhalation (T50) CT data for treatment planning and the calculation of the compensating bolus because the exhalation phase is more stable than the inhalation phase [22, 23]. Since bowel gas position could not be remained stable over 20 fractions, the HU number of bowel gas ( $\approx -100$  HU) was replaced by water equivalent HU (0 HU) to avoid undershooting for the PTVs. Dose distributions for all respiratory phases were then calculated using the original 4DCT (bowel gas region was not replaced). The compensating bolus was applied to a smearing algorithm to account for patient setup error and multiple scattering (calculation grid was  $3\text{ mm} \times 3\text{ mm}$ ). The smearing does not address the compensation of respiratory motion because our design compensating bolus has already accounted for it.

A multi-leaf collimator was used to define the field boundary for the PTV1/PTV2. All calculations were done using our in-house software, previously described in detail [24].

The prescribed dose was 66 GyE (3.3 GyE–20 fractions) delivered in two treatment courses. For the first treatment course, 33 GyE was delivered to PTV1 from the anterior (four fractions) and lateral directions (three fractions for each side). The second treatment course delivered the remaining 33 GyE to PTV2 from the lateral directions only (five fractions from the left and right side respectively, see

also (Fig. 1b). According to the definitions of PTV1 and PTV2, PTV1 and PTV2 should be irradiated at 50% and 100% of the total prescribed dose, respectively.

We evaluated the prostate center of mass (COM) trajectory in a single respiratory motion. The dose delivery was assessed by the analysis of dose-volume histograms (DVHs) for the prostate, CTV, PTV1, PTV2 and the rectum. Further, the dose received by a volume greater than 95% (D95) for the prostate and PTV2, as well as the rectum volume irradiated with more than 30 GyE and 60 GyE (V30 and V60), were calculated.

## RESULTS

### Prostate motion

The displacement of the prostate COM over a single respiration was observed to be less than 0.7 mm (Table 1). COM displacement was considerably larger in posterior, superior and inferior directions than in the other directions (Table 2). The IM was calculated as the maximum distance from the edge of the CTV based on the 4DCT data (Table 2). It was less than 1.6 mm during a single respiratory phase.

### Abdominal thickness

The abdominal thickness variation map ( $T_n$  minus T50) for Patient no. 6 was increased around inhalation phase (Fig. 2, upper panel). Although the prostate COM displacement was very small ( $= 0.2\text{ mm}$ ), the mean variation was  $1.5 \pm 1.0\text{ mm-WEL}$  for ROI1,  $2.9 \pm 0.5\text{ mm-WEL}$  for ROI2, and  $0.5 \pm 0.4\text{ mm-WEL}$  for ROI3. Over 3 mm-WEL variation was observed on the anterior side of ROI1 due to respiratory-induced abdominal thickness variation. These variations over ROI1 were determined via an analysis of the histogram of these images at the respective phases (Fig. 3a). The abdominal thickness variation area was

**Table 2.** Prostate center of mass displacement and internal margin averaged over all patients in a single respiration

		Unit:mm					
		Left	Right	Anterior	Posterior	Superior	Inferior
Prostate COM	Mean	0.1	0.0	0.0	0.2	0.1	0.1
	Range	0.0–0.2	0.0–0.2	0.0–0.2	0.0–0.5	0.0–0.7	0.0–0.5
	s.d.	0.1	0.1	0.1	0.1	0.2	0.1
Internal margin	Mean	0.2	0.1	0.0	0.3	0.1	0.4
	Range	0.0–1.6	0.0–0.0	0.0–0.0	0.0–1.6	0.0–1.0	0.0–1.0
	s.d.	0.4	0.3	0.0	0.6	0.3	0.5

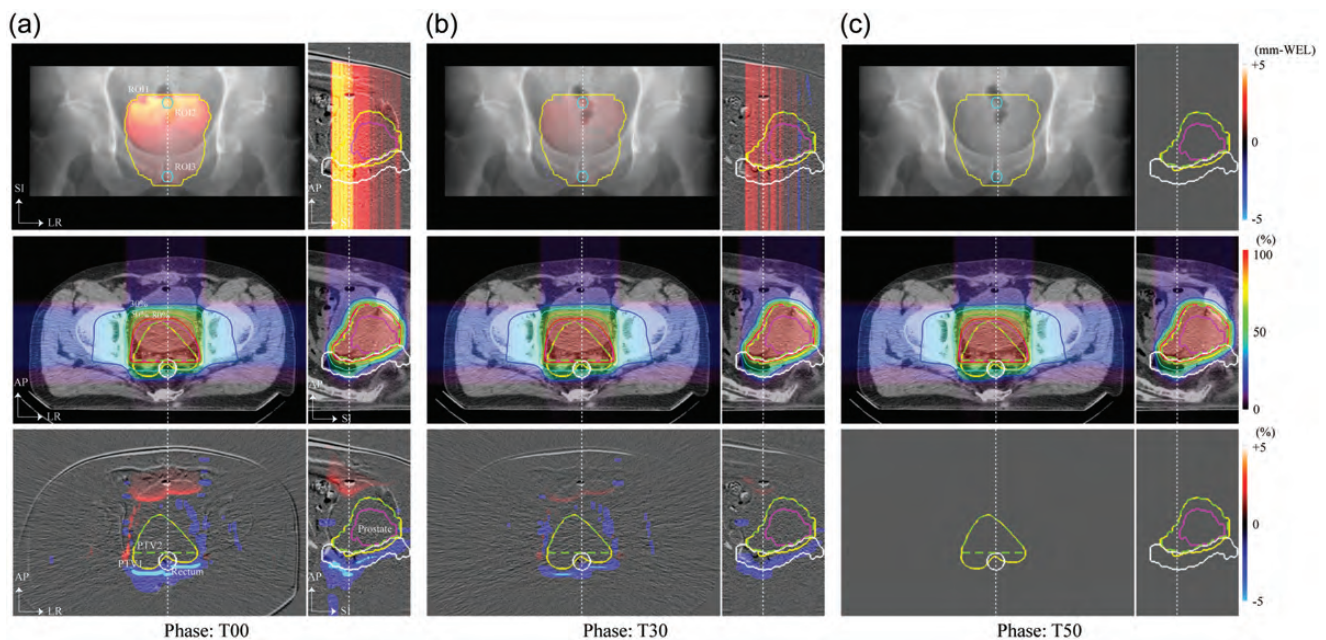


**Fig. 2.** Selected dose assessment images for Patient no. 6. Panels (a)–(c) show the abdominal thickness variation (upper row) between the CT phases  $T_n$ –T50, the dose distribution for the CT phase  $T_n$  (middle row) and the dose difference (lower row)  $T_n$ –T50 for the CT phase  $T_n = T00$  (peak-inhalation), T30 (mid-exhalation) and T50 (peak-exhalation), respectively. Each panel (a)–(c) consist of two views as indicated by the axis in the lower left corner of the figures of panel (a). On the left hand-side (coronal section) of the upper row the various ROI's are contoured, namely, ROI1 (yellow), ROI2/3 (light blue), additionally they are labeled only in panel (a). On the right-hand-side figure of each panel (a)–(c) the contour of the prostate (purple), rectum (white), PTV1 (yellow) and PTV2 (light blue) are drawn. On the middle row, additionally, the dose contours are superimposed using the following labeling: 95% (pink), 90% (red), 80% (green), 50% (light blue) and 30% (blue). ROI=region of interest, CTV=clinical target volume, PTV=planning target volume, AP=anterior-posterior.

increased in the inhalation phase. An abdominal thickness variation over 3 mm-WEL is observed in  $1523 \text{ mm}^2$  at T00.

For another patient (Patient no. 12) the abdominal thickness variation was smaller than that in the previous case ( $0.5 \pm 0.8 \text{ mm-WEL}$ ,  $0.7 \pm 0.4 \text{ mm-WEL}$ , and  $0.3 \pm 0.3 \text{ mm-WEL}$  for ROI1, ROI2 and ROI3, respectively). However, hot and cold spots (approximately  $\pm 5 \text{ mm-WEL}$ ) were observed. These were caused by rectum gas movements (Fig. 4, upper panel). A histogram of the abdominal

thickness variation is shown in Fig. 5a. The abdominal thickness variation area was increased for the inhalation phase. An abdominal thickness variation of over 3 mm-WEL was observed in  $92 \text{ mm}^2$  at T00. The variations in T30 and T40 were about the same.

The variations of the abdominal thickness averaged over all patients were  $0.7 \pm 0.6 \text{ mm-WEL}$  for ROI1,  $1.2 \pm 0.4 \text{ mm-WEL}$  for ROI2 and  $0.3 \text{ mm} \pm 0.4 \text{ mm-WEL}$  for ROI3 (Table 3). For three patients (Patient nos. 11, 12 and 14)

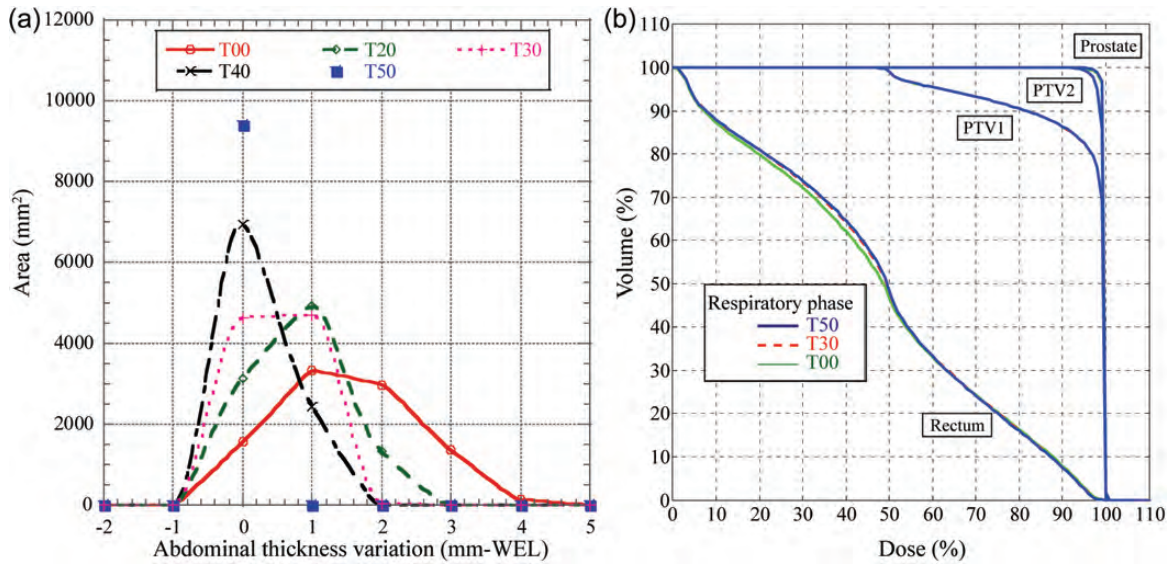


**Fig. 3.** (a) Histogram of abdominal thickness variation in ROI1 for Patient no. 6. (b) DVHs for prostate, rectum, PTV1 and PTV2 at peak-inhalation (T00), mid-exhalation (T30) and peak-exhalation (T50). DVH = dose volume histogram, WEL = water equivalent length, CTV = clinical target volume, PTV = planning target volume.

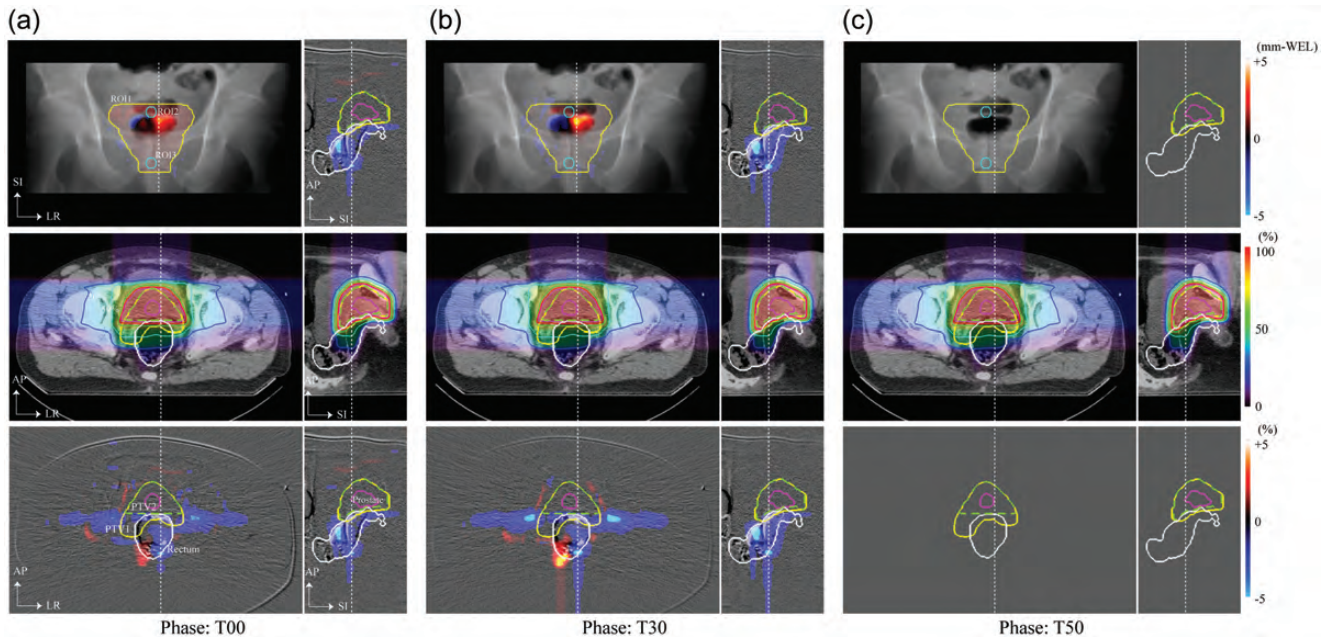


**Fig. 4.** Selected dose assessment images for Patient no. 12. Panels (a)–(c) show the abdominal thickness variation (upper row) between the CT phases  $T_n$ –T50, the dose distribution for the CT phase  $T_n$  (middle row) and the dose difference (lower row)  $T_n$ –T50 for the CT phase  $T_n = T00$  (peak-inhalation), T30 (mid-exhalation) and T50 (peak-exhalation), respectively. Each panel (a)–(c) consist of two views as indicated by the axis in the lower left corner of the figures of panel (a). On the left hand-side (coronal section) of the upper row the various ROI's are contoured, namely, ROI1 (yellow) and ROI2/3 (light blue); additionally they are labeled only in panel (a). On the right-hand-side figure of each panel (a)–(c) the contour of the prostate (purple), rectum (white), PTV1 (yellow) and PTV2 (light blue) are drawn. On the middle row, additionally, the dose contours are superimposed using the following labeling: [95% (pink), 90% (red), 80% (green), 50% (light blue) and 30% (blue)]. ROI = region of interest, CTV = clinical target volume, PTV = planning target volume, AP = anterior-posterior.

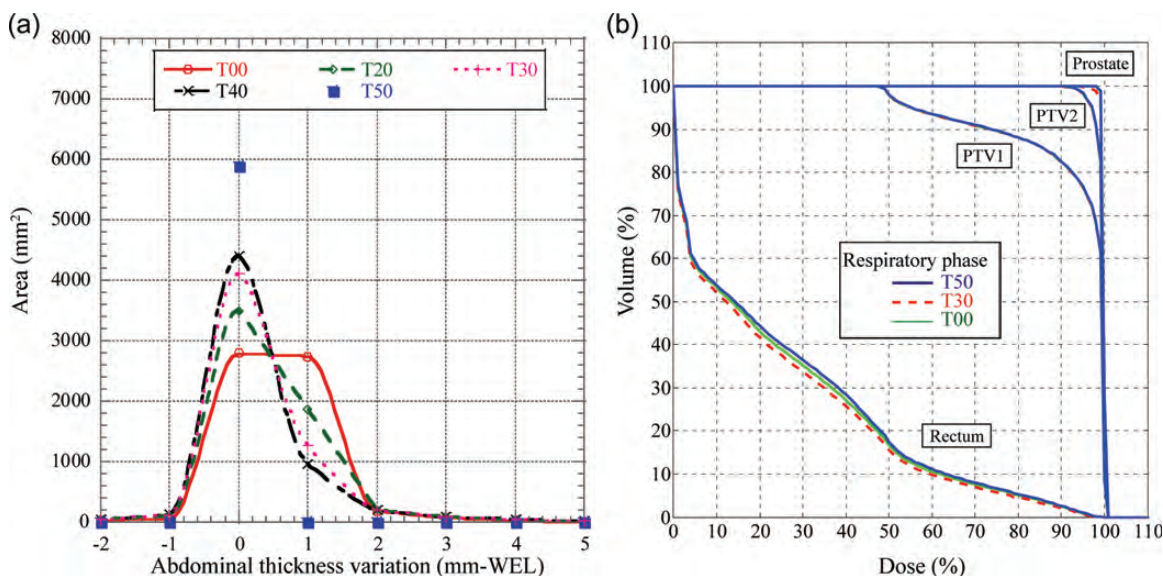


**Fig. 5.** (a) Histogram of abdominal thickness variation in ROI1 for Patient no. 12. (b) DVHs for prostate, rectum, PTV1 and PTV2 at peak-inhalation (T00), mid-exhalation (T30) and peak-exhalation (T50). DVH = dose volume histogram, CTV = clinical target volume, PTV = planning target volume.

variations larger than over 5 mm-WEL were observed. The maximum and minimum values within the ROIs are based on a pixel-by-pixel analysis. Hence even a single high/low pixel value will result in a high/low maximum/minimum but this would have no effect on the dose distribution due to range straggling and multi-coulomb scattering.

### Dose assessment

For Patient no. 6, carbon-ion beam dose distributions at T00, T30 and T50 are shown in Fig. 2 (middle panel). The doses to the prostate, CTV, PTV1 and PTV2 were unchanged, however, the dose to the rectum changed with the respiratory phases, particularly for the cephalad parts of PTV1. This is due to the abdominal thickness variation, as described above. As a result, the spread out Bragg peak (SOBP) position was shifted towards the proximal side. A part of the rectum was included in the SOBP because the rectum was enclosed by the shape of the PTV1. To simplify the understanding of this dose variation, we visualized the subtracted doses ( $T_n$  minus T50) as shown in Fig. 2 (lower panel). The axial planes show the slices of the seminal vesicle and the bladder (above the prostate). While underdosage was observed on the posterior side of the PTV1, which decreased the rectum dose, overdosage to the anterior side of the PTV1 was observed. The dose variation on the lateral sides was smaller than that on the posterior side. The magnitude of the dose variation was more significant on the cephalad side of the PTV1 than the caudal side due to abdominal thickness variation. Overdosages were observed on the right side of the PTV1, which was

caused by the left side of abdominal thickness variation around inhalation (Fig. 2a, lower panel).

The DVHs for prostate, CTV, PTV1, PTV2 and rectum at T00, T30 and T50 are shown in Fig. 3b for the same patient (Patient no. 6). D95 values for prostate, CTV, PTV1 and PTV2 were 98.0%, 95.2%, 61.2% and 97.0% averaged over all respiratory phases. From the rectum DVH we can see that rectal dose below a dose of 50% was slightly smaller for T00 compared to T30 and T50. The DVH above a dose of 50% is the same for all phases.

For Patient no.12, dose distributions at T00, T30 and T50 are shown in Fig. 4 (middle panel). The dose to the target did not change for the different phases, however, the dose variation to the rectum was larger than that in the previous case due to rectum gas movement (Fig. 4, lower panel). The DVH curves were overlapped at all individual respiratory phases for prostate, CTV, PTV1, PTV2 and rectum for Patient No. 12 (Fig. 5b). D95 values of prostate, CTV, PTV1 and PTV2 were 98.0%, 81.9%, 54.1% and 96.1% for all respiratory phases, respectively.

For all patients, D95 values for the CTV, PTV1 and PTV2 were over 69.9%, 54.0% and 95.1%, respectively (Fig. 6 and Table 4). V60 and V30 values for the rectum were less than 8.0% and 59.7%, respectively. Mean D95 values for the prostate and PTV2 were 97.7%. The D95 for CTV and PTV1 were not always over 90% of the prescribed dose. This was because the PTV1 includes the part of the CTV which was cut to avoid the rectum dose in the first ten fractions of the treatment course. Moreover, for the CTV the volume and position could change as a function of respiratory motion as compared to the PTV1, which is

**Table 3.** Abdominal thickness variations for all patients in ROI1, ROI2 and ROI3

Pt .no	Unit:WEL-mm		
	ROI1 mean $\pm$ s.d.	ROI2 mean $\pm$ s.d.	ROI3 mean $\pm$ s.d.
1	0.8 $\pm$ 0.4	1.2 $\pm$ 0.4	0.6 $\pm$ 0.3
2	0.7 $\pm$ 0.7	1.5 $\pm$ 0.4	0.1 $\pm$ 0.2
3	0.5 $\pm$ 0.5	1.1 $\pm$ 0.4	0.0 $\pm$ 0.1
4	2.4 $\pm$ 0.6	2.9 $\pm$ 0.4	1.8 $\pm$ 0.4
5	0.7 $\pm$ 0.4	1.1 $\pm$ 0.4	0.4 $\pm$ 0.4
6	1.5 $\pm$ 1.0	2.9 $\pm$ 0.5	0.5 $\pm$ 0.4
7	0.6 $\pm$ 0.4	0.8 $\pm$ 0.3	0.4 $\pm$ 0.4
8	0.9 $\pm$ 0.5	1.7 $\pm$ 0.6	0.5 $\pm$ 0.4
9	0.3 $\pm$ 0.4	0.8 $\pm$ 0.4	0.1 $\pm$ 0.2
10	0.7 $\pm$ 0.5	1.0 $\pm$ 0.4	0.4 $\pm$ 0.4
11	0.6 $\pm$ 1.2	1.2 $\pm$ 0.7	0.0 $\pm$ 0.2
12	0.5 $\pm$ 0.8	0.7 $\pm$ 0.4	0.3 $\pm$ 0.3
13	0.5 $\pm$ 0.6	1.3 $\pm$ 0.4	0.1 $\pm$ 0.3
14	0.9 $\pm$ 0.6	1.1 $\pm$ 0.5	0.5 $\pm$ 0.4
15	0.0 $\pm$ 0.2	0.2 $\pm$ 0.3	0.0 $\pm$ 0.2
16	0.1 $\pm$ 0.3	0.3 $\pm$ 0.5	0.1 $\pm$ 0.3
17	0.8 $\pm$ 0.6	1.5 $\pm$ 0.3	0.2 $\pm$ 0.3
18	0.5 $\pm$ 0.4	0.7 $\pm$ 0.4	0.4 $\pm$ 0.4
19	0.1 $\pm$ 0.4	0.1 $\pm$ 0.2	0.0 $\pm$ 0.2
20	0.5 $\pm$ 0.5	1.2 $\pm$ 0.4	0.3 $\pm$ 0.3
Mean	0.7 $\pm$ 0.6	1.2 $\pm$ 0.4	0.3 $\pm$ 0.3

Pt. no. = patient number, ROI = region of interest, WEL = water equivalent path length, SD = standard deviation.

not changed. A small dose difference was found regarding V30 for the rectum, which was caused by the dose difference around the PTV1. An even smaller difference was found for V60.

## DISCUSSION

In this study we quantified intrafractional prostate motion and its impact on the carbon-ion beam dose variation by using 4DCT information. We found that the prostate displacement was less than 0.7 mm in a single respiratory cycle, and the effect of respiration on the dose distribution to the targets (prostate, PTV1 and PTV2) was small, however, the dose to the rectum varied according to the abdominal thickness.

## Intrafractional motion

Our results clearly showed that the intrafractional prostate motion is small. This supports our prostate treatment protocol without respiratory gating. The obtained values for prostate intrafractional motion are smaller than the voxel size of the 4DCT. Since delineating the prostate based on CT images is more difficult than using MRI or ultrasound images [19], contouring errors could occur. To minimize these errors MRI images were used as additional guidance while contouring, and the error from miscountering of the prostate was minimized because it was obtained by averaging over all prostate voxel positions.

Kitamura *et al.* reported that approximately 2 cm prostate motion was observed in the prone position over a 2 min observation due to bowel movement. Based on this, they advised that treatment beam-on time in intensity-modulated radiotherapy should be shortened [4]. Since the treatment beam-on time in carbon-ion beam therapy at NIRS is less than 2 min, the probability of bowel movement is expected to be small.

## Dose variation

Our results showed that respiratory-induced dose variations were negligible, which agreed with the findings of several other reports published on respiratory-induced prostate dose variation in photon beam treatment [9, 10]. The good dose preservation to the target was firstly attributed to the very small prostate COM displacement (under 1 mm). Secondly, the density of the tissue around the prostate is more solid when compared to the lung region, hence, the treatment beam overshoot and undershoot that were caused by the organ motion were small. This is also one of the factors limiting the accuracy of volume contouring. In general, drawing the exact same contour of a volume is very difficult. Fiorio *et al.* reported that the intra-observer variability in contouring the prostate has been found to be quite small and should have no significant effects on conformal treatment planning [25]. To improve the contouring accuracy, we used the fast rotation conebeam CT (256MSCT) for providing good quality imaging compared with the conventional MSCT. The merit of using the 256MSCT is having the 4DCT artifact, as observed in the conventional MSCT [26]. The resolution of superior-inferior direction was good because we used a slice thickness of 1 mm. From the results of the dose difference shown in Fig. 2, the variation of abdominal thickness could be estimated to be the main factor for the dose difference in particle therapy. A sufficient dose was irradiated to the prostate, and an underdose was received on the posterior side of the PTV1. It was because the thickness of the abdomen increased at the peak-inhalation phase compared to the treatment planning (peak-exhalation phase). This point is much more

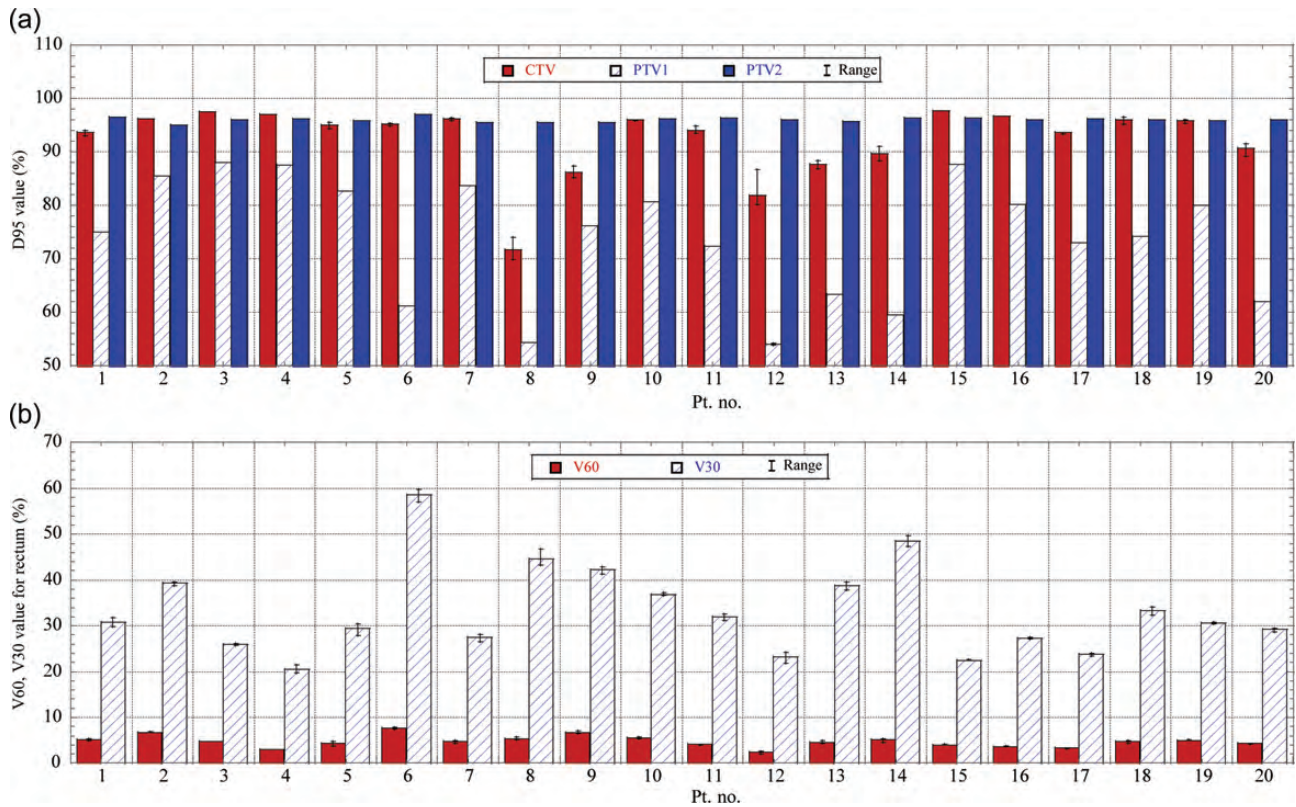


**Fig. 6.** Dose assessment overview results for all patients. (a) D95 values for CTV, PTV1 and PTV2, average value and variation range over all phases. (b) V60 and V30 mean values for rectum in all phases (V30/V60 = volume receiving an irradiating over 30/60 GyE). Pt. no. = patient number, CTV = clinical target volume, PTV = planning target volume.

**Table 4.** Dose assessment (D95 for prostate, CTV, PTV1, PTV2 and V60/V30 for the rectum) averaged over all patients

Metrics		mean $\pm$ s.d.	(Range)
Prostate	D95 (%)	97.7 $\pm$ 0.4	(97.0–98.1)
CTV	D95 (%)	92.5 $\pm$ 6.5	(69.9–97.8)
PTV1	D95 (%)	74.1 $\pm$ 11.3	(54.0–88.1)
PTV2	D95 (%)	96.1 $\pm$ 0.4	(95.1–97.0)
Rectum	V60 (%)	4.8 $\pm$ 1.3	(2.1–8.0)
	V30 (%)	33.3 $\pm$ 9.7	(19.8–59.7)

CTV, PTV1 and PTV2 are defined as shown in Fig. 1. CTV = clinical target volume, PTV = planning target volume, SD = standard deviation.

important in particle therapy than photon therapy due to the pronounced range of charged particles.

The dose to the rectum would be changed by the abdominal thickness variation of the anterior beam direction. However, 4 of the total 20 irradiation fractions were from the anterior direction; lateral beams accounted for the other 16 irradiated fractions. For Patient no. 12, the rectal volume

received < 50% of prescribed doses at T00 and T30, which were smaller compared with that of T50. This was because the dose variation due to the abdomen thickness variation occurred only around the PTV1. Therefore, the rectum DVH was lower at a prescribed dose over 50% and no change was observed for the different respiratory phases. Moreover, the rectum dose was lower than for Patient no.6. This was because the positions of the PTV1 and rectum were not in proximity. The PTV2 was similar to the PTV1, because the cutline volume of the PTV1 was small. The magnitude of the inter-patient variation of the DVH may be larger than the variation caused by intrafractional changes. However, that is beyond the aim of this study. In this study, the prescribed dose from the anterior direction delivered only 20% of the total prescribed dose. The effect of that appears limited to a slight increase in the rectal V30 and V60. However, the treatment beam from the anterior direction was often used to avoid the rectum dose in other multiple-portal therapy, which could possibly cause rectal toxicity.

The treatment protocol in our institute uses two fixed beam ports (horizontal and vertical). The patient bed must be able to rotate (roll) for irradiations at oblique beam angles. Then, the dose to the rectum will increase when the

treatment beam is incident from the posterior direction. According to the results of the dose difference for the anterior beam direction, the treatment accuracy would be improved by neglecting this beam direction.

### Gas bowel movement

Intrafractional rectum gas movement is another factor affecting the dose distribution. However, since we tried to remove the rectum gas and applied a bowel filling, the impact of this dose degradation was small. Our group found similar difficulties in the case of pancreas treatment with significant degradation of the dose conformation to the target, even under consideration of respiratory phases [27]. A possible solution to this problem is a real-time control of the beam delivery guided by a real-time monitoring of the gas bowel using X-ray images or ultrasound.

### Accumulated dose assessment

Dosimetric assessment by using the accumulated dose along the time axis, which is considered the probability density function of organs and organ deformation, is necessary in clinical practice to reduce very time-consuming dose assessment as a function of respiratory phase. We evaluated the rectum dose for each respiratory phase independently. The analysis showed that this was not significantly different from the treatment planning dose distribution (T50). We did not calculate the accumulated dose by using deformable image registration (DIR), because as Brock *et al.* showed [28], the error of DIR in the abdominal region is about 2.5 mm when using 4DCT. The spatial resolution of CT images is one of the factors that affects the deformable image registration accuracy. Because the spatial resolution in our 4DCT was higher than Brock's, and the intrafractional prostate motion in our study was equal to or smaller than the deformable image registration inaccuracy, we did not use DIR, hence, the evaluated dose distributions at each respiratory phase. Further, the respiratory ungated prostate treatment using the 3D uniform margin for the CTV provided a sufficient dose to the prostate and to the PTV2.

### Study limitations

Several limitations of this study warrant mention. One limitation is the 4DCT scan time, which is set to acquire only a single respiratory cycle, because we wanted to minimize the patient radiation dose. Further, most treatment facilities require several minutes to irradiate a target volume, but not so ours. Therefore, we have no information on the respiratory pattern variation (phase shift/phase drift [29]).

Another limitation is that we did not evaluate interfractional motion. Several studies have reported that the magnitude of prostate intrafractional motion is smaller than interfractional motion [5, 8]. Rectum gas movement is an important factor inducing interfractional prostate motion, as well as

intrafractional motion [30]. We focused on intrafractional motion in this study, therefore, treatment uncertainty due to interfractional changes should be examined in a future study.

## CONCLUSION

Doses to the prostate, PTV1 and PTV2 were not significantly affected by respiration, however, a respiratory-induced abdominal thickness change was identified as a factor affecting dose variation, even though the prostate motion was small (<0.7 mm). It is important to consider the geometrical changes from the beam entrance to the target as well as the target motion, especially in particle therapy.

## REFERENCES

1. Bragg W, Kleeman R. On the ionisation curves of radium. *Phil Mag* 1904;**8**:726–38.
2. Ishikawa H, Tsuji H, Kamada T *et al.* Carbon-ion radiation therapy for prostate cancer. *Int J Urol* 2012;**19**:296–305.
3. Adamson J, Wu Q. Prostate intrafraction motion evaluation using kV fluoroscopy during treatment delivery: a feasibility and accuracy study. *Med Phys* 2008;**35**:1793–806.
4. Kitamura K, Shirato H, Seppenwoolde Y *et al.* Three-dimensional intrafractional movement of prostate measured during real-time tumor-tracking radiotherapy in supine and prone treatment positions. *Int J Radiat Oncol Biol Phys* 2002;**53**:1117–23.
5. Mah D, Freedman G, Milestone B *et al.* Measurement of intrafractional prostate motion using magnetic resonance imaging. *Int J Radiat Oncol Biol Phys* 2002;**54**:568–75.
6. Ghilezan MJ, Jaffray DA, Siewerdsen JH *et al.* Prostate gland motion assessed with cine-magnetic resonance imaging (cine-MRI). *Int J Radiat Oncol Biol Phys* 2005;**62**:406–17.
7. Langen KM, Willoughby TR, Meeks SL *et al.* Observations on real-time prostate gland motion using electromagnetic tracking. *Int J Radiat Oncol Biol Phys* 2008;**71**:1084–90.
8. Xie Y, Djajaputra D, King CR *et al.* Intrafractional motion of the prostate during hypofractionated radiotherapy. *Int J Radiat Oncol Biol Phys* 2008;**72**:236–46.
9. Zhang X, Dong L, Lee AK *et al.* Effect of anatomic motion on proton therapy dose distributions in prostate cancer treatment. *Int J Radiat Oncol Biol Phys* 2007;**67**:620–9.
10. Miralbell R, Ozsoy O, Pugliesi A *et al.* Dosimetric implications of changes in patient repositioning and organ motion in conformal radiotherapy for prostate cancer. *Radiother Oncol* 2003;**66**:197–202.
11. Murphy MJ. Tracking moving organs in real time. *Semin Radiat Oncol* 2004;**14**:91–100.
12. Furukawa T, Inaniwa T, Sato S *et al.* Design study of a raster scanning system for moving target irradiation in heavy-ion radiotherapy. *Med Phys* 2007;**34**:1085–97.
13. Bert C, Gemmel A, Saito N *et al.* Gated irradiation with scanned particle beams. *Int J Radiat Oncol Biol Phys* 2009;**73**:1270–5.
14. Kanematsu N, Endo M, Futami Y *et al.* Treatment planning for the layer-stacking irradiation system for three-dimensional

- conformal heavy-ion radiotherapy. *Med Phys* 2002;**29**:2823–9.
15. Endo M, Mori S, Tsunoo T *et al.* Development and performance evaluation of the first model of 4D CT-scanner. *IEEE Trans Nucl Sci* 2003;**50**:1667–71.
  16. Mori S, Endo M, Tsunoo T *et al.* Physical performance evaluation of a 256-slice CT-scanner for four-dimensional imaging. *Med Phys* 2004;**31**:1348–56.
  17. Olsen JR, Lu W, Hubenschmidt JP *et al.* Effect of novel amplitude/phase binning algorithm on commercial four-dimensional computed tomography quality. *Int J Radiat Oncol Biol Phys* 2008;**70**:243–52.
  18. Wink N, Panknin C, Solberg TD. Phase versus amplitude sorting of 4D-CT data. *J Appl Clin Med Phys* 2006;**7**:77–85.
  19. Roach M, III, Faillace-Akazawa P, Malfatti C *et al.* Prostate volumes defined by magnetic resonance imaging and computerized tomographic scans for three-dimensional conformal radiotherapy. *Int J Radiat Oncol Biol Phys* 1996;**35**:1011–8.
  20. Rasch C, Barillot I, Remeijer P *et al.* Definition of the prostate in CT and MRI: a multi-observer study. *Int J Radiat Oncol Biol Phys* 1999;**43**:57–66.
  21. Tsuji H, Yanagi T, Ishikawa H *et al.* Hypofractionated radiotherapy with carbon ion beams for prostate cancer. *Int J Radiat Oncol Biol Phys* 2005;**63**:1153–60.
  22. Kubo HD, Len PM, Minohara S *et al.* Breathing-synchronized radiotherapy program at the University of California Davis Cancer Center. *Med Phys* 2000;**27**:346–53.
  23. Vedam SS, Keall PJ, Kini VR *et al.* Determining parameters for respiration-gated radiotherapy. *Med Phys* 2001;**28**:2139–46.
  24. Mori S, Chen GT. Quantification and visualization of charged particle range variations. *Int J Radiat Oncol Biol Phys* 2008;**72**:268–77.
  25. Fiorino C, Reni M, Bolognesi A *et al.* Intra- and inter-observer variability in contouring prostate and seminal vesicles: implications for conformal treatment planning. *Radiother Oncol* 1998;**47**:285–92.
  26. Yamamoto T, Langner U, Loo BW, Jr *et al.* Retrospective analysis of artifacts in four-dimensional CT images of 50 abdominal and thoracic radiotherapy patients. *Int J Radiat Oncol Biol Phys* 2008;**72**:1250–8.
  27. Kumagai M, Hara R, Mori S *et al.* Impact of intrafractional bowel gas movement on carbon ion beam dose distribution in pancreatic radiotherapy. *Int J Radiat Oncol Biol Phys* 2009;**73**:1276–81.
  28. Brock KK. Results of a multi-institution deformable registration accuracy study (MIDRAS). *Int J Radiat Oncol Biol Phys* 2010;**76**:583–96.
  29. Keall PJ, Mageras GS, Balter JM *et al.* The management of respiratory motion in radiation oncology report of AAPM Task Group 76. *Med Phys* 2006;**33**:3874–900.
  30. Ogino I, Uemura H, Inoue T *et al.* Reduction of prostate motion by removal of gas in rectum during radiotherapy. *Int J Radiat Oncol Biol Phys* 2008;**72**:456–66.